*J. Fluid Mech.* (2012), *vol.* 709, *pp.* 106–122.  
doi:10.1017/jfm.2012.323

# Subcritical transition and spiral turbulence in circular Couette flow

**M. J. Burin† and C. J. Czarnocki**

Department of Physics, California State University San Marcos, CA 92096, USA

(Received 10 August 2011; revised 1 June 2012; accepted 25 June 2012;
first published online 21 August 2012)

We present new observations of a controlled transition to turbulence in a fundamental but little-studied regime: circular Couette flow with only the outer cylinder rotating. Our apparatus consists of an outer cylinder of fixed radius and three inner cylinders having different radii that are used interchangeably to study the effect of flow curvature. With the smallest inner cylinder the end-cap configuration (vertical boundary conditions) may also be varied. The turbulent transition is found to be sensitive to both gap width and end-cap configuration, with wider gaps transitioning at higher rotation rates. All configurations are observed to transition with hysteresis and intermittency. A laser Doppler velocimetry (LDV)-based study of the azimuthal velocity profile as a function of gap width and rotation rate reveals that turbulence, once initiated, is confined to regions of significant shear. For wider gap widths, the radial location of these shear layers is determined by the chosen end-cap configuration. This, in turn, affects the transition Reynolds number, which we posit to be radially dependent. The narrow-gap case in particular features spiral turbulence, whose properties are found to be similar to observations of the phenomenon in related shear flows. The velocity profile in this case is correlated with overlapping boundary layers, suggesting a coupling mechanism for the origin of laminar-turbulent banding phenomena.

**Key words:** shear layer turbulence, Taylor–Couette flow, transition to turbulence

## 1. Introduction

Given the large and diverse number of studies on circular Couette flow during the past century, it is perhaps surprising to note that the case of the transition to turbulence solely due to outer cylinder rotation has received only occasional attention. It is well known that the transition to turbulence with the inner cylinder rotating occurs via a linear (Taylor) instability that sets in above a viscous threshold at Reynolds numbers ($Re$) near $10^2$. The Reynolds number $Re$ in this system may be evaluated as

$$Re = \frac{\Delta\Omega R \Delta R}{\nu} \tag{1.1}$$

where $\Delta\Omega$ is the difference in rotation rate between the two cylinders (which for the experiments reported here is just the outer cylinder rotation rate or $\Omega_o$), $\Delta R$ is the annular gap width ($R_o - R_i$); $R$ represents either the inner ($i$) or outer cylinder ($o$)

† Email address for correspondence: mburin@csusm.edu

radius (we use the latter), and $\nu$ is the kinematic viscosity of the fluid. System geometry is typically summarized by the radius ratio $\eta = R_i/R_o$ and aspect ratio $\Gamma = H/\Delta R$, where $H$ is the axial height of the annulus. Supercritical instability initially takes the form of toroidal vortices which advectively relax the imposed angular momentum gradient (Taylor 1923). With increasing $Re$, a fascinating sequence of bifurcations and modal evolution ensues until a fully turbulent state is ultimately reached at sufficiently high $Re$ ($\leqslant 10^6$), with the exact value depending on $\eta$.

In contrast to the supercritical transition described above, a subcritical transition may be observed in the case of counter-rotating cylinders. In such flows a radial region near the inner cylinder is linearly unstable according to the Taylor criterion but, past a null velocity circumference in radius, one encounters a linearly stable flow that extends outward in radius to the outer cylinder. Turbulent features seen in counter-rotating flows may differ greatly from when only the inner cylinder rotates. In fact, fully developed turbulence can appear abruptly in $Re$ space, leading to the term 'catastrophic' transition (Coles 1965). This transitional state has been observed to be highly intermittent in both space and time. It is presumed that instability in the outer layer is triggered from unstable motions caused by the linear instability penetrating outwards past the null point, which serve as finite-amplitude perturbations (Coughlin & Marcus 1996).

The $(Re_i, Re_o)$ parameter space explored in Taylor–Couette flow (i.e. $Re$ based on $\Omega_i$ and $\Omega_o$, respectively) has recently been expanded by Paoletti & Lathrop (2011) and van Gils *et al.* (2011), who have independently found momentum flux (torque) scaling in the strongly turbulent regime corresponding to theory developed by Eckhardt, Grossmann & Lohse (2007) in analogy to Rayleigh–Bérnard heat convection. This new work follows Dubrulle *et al.* (2005) in framing $(Re_i, Re_o)$ based on independently rotating cylinders as a single rotation number,

$$R_\Omega = \frac{(1-\eta)(Re_o + Re_i)}{\eta Re_o - Re_i} \tag{1.2}$$

which for the experiments presented here, where $Re_i = 0$, reduces to $(1-\eta)/\eta$. This expression may also be cast in terms of a Rossby number $Ro = (\Omega_i - \Omega_o)/\Omega_o$, which in our experiments, for all three cylinder radii, is a constant $Ro = -1$. In restricting this parameter our emphasis is intended to be on the subcritical transition process and in particular on velocimetry, for which there is a lack of data, although new work is now filling the gap (e.g. van Gils *et al.* 2011; van Hout & Katz 2011).

In counter-rotating flows a particularly fascinating intermediate subcritical state, spiral turbulence, has been observed. Featuring alternating oblique bands of laminar and turbulent flow, this state was first documented by Coles (1965) and van Atta (1966) and is a rich example of the complexity encapsulated within the Navier–Stokes equations. Later observations of spiral turbulence by others (such as Andereck, Liu & Swinney 1986; Hegseth *et al.* 1989; Prigent *et al.* 2002) in counter-rotating flows have added experimental details on this regime, and recent simulation efforts seem to be closing in on its fine-scale structure and mechanisms (Dong 2009; Meseguer *et al.* 2009; Dong & Zheng 2011). Recent simulations of the turbulent banding phenomenon in planar Couette flows are also making significant progress (e.g. Duguet, Schlatter & Henningson 2010; Tuckerman & Barkley 2011). This phenomenon has been observed also in two-dimensional Poiseuille flow (Hashimoto *et al.* 2009), rotating planar Couette flow (Tsukahara, Tillmark & Alfredsson 2010), and torsional Couette flow between a rotating and stationary disc (Cros & Le Gal 2002). The underlying physics describing this banded state has remained elusive, but theoretical progress has

been promising in recent years, e.g. with the Ginzberg–Landau framework of pattern formation being successfully applied (Prigent *et al.* 2002; Rolland & Manneville 2011).

The recent activity and emerging detail on the subcritical transition various wall-bounded shear flows is in marked contrast to the relatively little information that can be gleaned from early Taylor–Couette experiments on subcritical transition driven by pure outer cylinder rotation. Similarities with counter-rotating flows may be reasonably anticipated *a priori*, but experimental knowledge is nonetheless lacking.

Early experiments with the inner cylinder held stationary present to us a suggestive if incomplete picture of a subcritical transition to turbulence for sufficient outer cylinder speeds or $Re$ (Wendt 1933; Taylor 1936; Couette 1890; Mallock 1896). In contrast to the supercritical transition described above (as well as to counter-rotating flows), this regime is understood to be linearly stable throughout the entire annulus for all $Re$ (Joseph 1976). Thus, the transition to turbulence must be initiated by finite-amplitude perturbations inherent to the experimental apparatus or otherwise externally introduced, as in the planar Couette flow studied by Daviaud, Hegseth & Bergé (1992). In all earlier reports for this experimental arrangement the turbulence apparently develops immediately over an incremental step in $Re$. Many of these early findings are compiled in Richard & Zahn (1999), who noted, along with Zeldovich (1981), that above a narrow-gap (planar) limit the critical $Re$ for transition ($Re_{cr}$) for the cyclonic case (i.e. with shear and rotation vectors aligned throughout the bulk flow, achieved naturally with sole $\Omega_o$ rotation) appears to scale with the square of the normalized gap width. Scaling of $Re_{cr}$ in the anticyclonic case is still basically unknown, and it is apparently quite sensitive to end-cap effects (Ji *et al.* 2006).

Despite these significant early achievements, there remains some uncertainty inherent in the interpretation of the older data, and calls for modern data detailing the subcritical transition have been made (Dubrulle *et al.* 2005). Also, early studies typically utilized torque as the main diagnostic and, having opaque outer cylinders, spatial details on the transitioning flow were naturally integrated and went unnoticed. While Couette (1890) and Mallock (1896) observed the subcritical transition visually, the more complete studies of Wendt (1933) and Taylor (1936) did not (although Taylor eventually had a small window installed for viewing through his outer cylinder). On the other hand the careful study by Schultz-Grunow (1959) using interchangeable inner cylinders contains fine visual observations but no velocimetry. More recent work by Yamada & Imao (1986) and Richard (2001) includes both velocimetry and visual observations, but for only a single geometry. Lastly we note that while the seminal work on spiral turbulence by Coles (1965) and van Atta (1966) includes reference to spiral turbulence observations with only the outer cylinder rotating (made by a Mr Oguro), further details are not given.

In what follows we illustrate some features of the subcritical transition in cyclonic circular Couette flow using three different gap widths (or degrees of curvature, $\eta$). We then discuss the significance of localized shearing and the distinctive context of spiral turbulence.

## 2. Apparatus

Figure 1 shows a schematic of our experimental device. The large outer cylinder has a 20.95 cm inner diameter, while the three interchangeable inner cylinders (composed of anodized aluminum and with radii 11.43, 15.24 and 20.32 cm) have been chosen to span a range of curvature, yielding radius ratios of $\eta = 0.55, 0.73$ and $0.97$

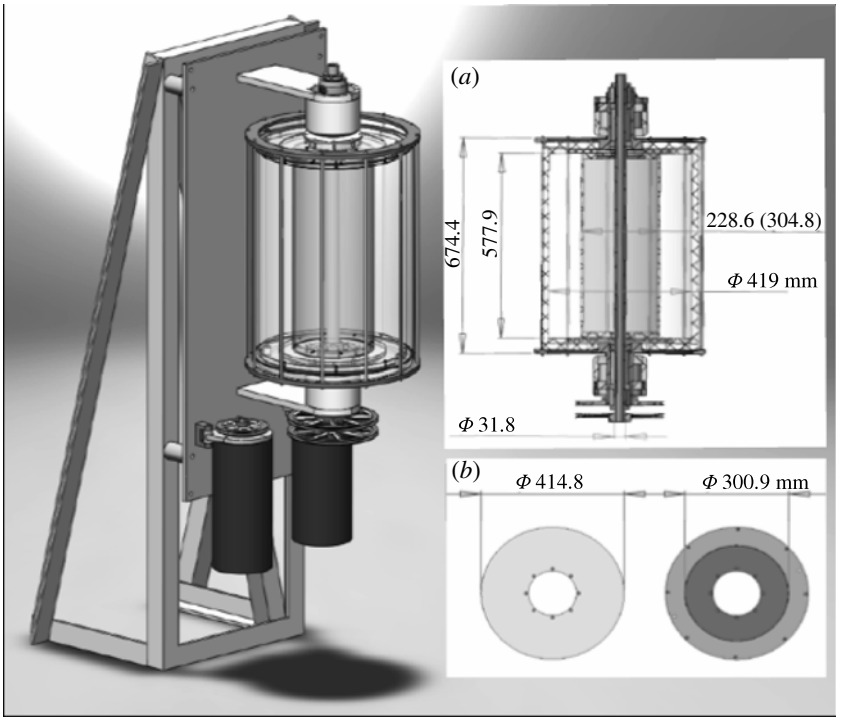


FIGURE 1. Experimental apparatus and its support structure. Dimensions are in millmetres. Inset (*a*) details the rotating vessel while inset (*b*) presents two possible end-cap configurations for the smallest inner cylinder ($\eta = 0.55$).

respectively. The working volume is about 60 cm tall, yielding aspect ratios ($\Gamma$) of 6, 10 and 92. Potentially high flow speeds necessitate somewhat thick (1.9 cm) acrylic walls to withstand relatively high dynamical pressures (up to 5 atmospheres).

The outer cylinder and vertical end plates of the apparatus are composed of a transparent cast acrylic to allow for both horizontal and vertical optical diagnostic access. Our current diagnostics include digital imaging (with 2–4 % Kalliroscope added by volume) and laser Doppler velocimetry (LDV). We used a Canon 7D CMOS-based camera adjacent to the apparatus for imaging. For LDV, the probe head is located on top of the apparatus on a radial traverse pointed downward (i.e. parallel to the axis of rotation), allowing for straightforward radial profiles of azimuthal velocity.

Both the inner and outer cylinders of the new apparatus are powered by one horsepower (0.75 kW) DC motors and can reach rotation rates near 15 rev $s^{-1}$. Combined with the relatively large dimensions of the device, *Re* of order $10^6$ (using water at room temperature) can thus be reached using the smallest inner cylinder/largest gap ($\eta = 0.55$). In the experiments discussed here *Re* is increased in increments of $\leqslant$0.3 Hz. This increment is considered adequately quasi-static in that smaller increments did not appear to affect the flow, but larger increments sometimes introduced observable perturbations, even turbulence, usually emanating from the end-caps.

With few exceptions, the end-caps of most similar devices are permanently connected to the outer cylinder. The design of this apparatus is intended to be more versatile, and features independent end-caps that may be split when in use with

the smallest inner cylinder. That is, they are composed of two annular sections that may be coupled to either cylinder, individually or coupled together. This versatility has a purpose: boundary-driven secondary flows may perturb the primary flow and inadvertently trigger instability (Lesur & Longaretti 2005). By varying end-cap conditions, the role of such secondary flows may be assessed and mitigated, as in Burin *et al.* (2006) and Schartman, Ji & Burin (2009).

There are two possible sources of uncertainty in $Re$ that are potentially significant. First, the apparatus was initially designed for high-speed operations and the controls are not optimized for lower speeds. As a consequence, at the lowest $Re$ reported here ($\approx$2000) there is an approximate 4–8 % uncertainty due to rotation fluctuations. This uncertainty is only an issue using the largest inner cylinder or smallest gap size ($\eta = 0.97$), and by $Re = 4500$ (near where we observe transition) it is down to 1–2 %, which is the maximum level of rotational uncertainty in $Re$ when using the other two cylinders (i.e. with wider gaps) for all $Re$ reported here. Second, the fluid is not actively temperature controlled, allowing for viscosity to be affected. Temperature was monitored during typical run times ($\leqslant$2 h) and changes to the water temperature were observed to be $<$2°C, leading to an additional uncertainty in $Re$ of $<$4 %. Such mild heating at relatively high $Re$ is perhaps counterintuitive. We suppose it is due to two causes: the first is that the inner cylinder of the apparatus is hollow and filled with water, which acts as a temperature ballast; the other is that shearing (and thus heating) largely takes place in a localized region and not throughout the whole annulus (discussed below). Considering these effects jointly, the $Re$ reported in the following observations are usually understood to be $<$5 % unless otherwise noted.

## 3. Observations

### 3.1. *Visual observations*

All flow configurations are observed to undergo a turbulent transition by increasing $Re$ via outer cylinder rotation, although details of the transition differ significantly with gap width or $\eta$. We first address $Re_{cr}$ for increasing $Re$ with respect to normalized gap width. Figure 2 presents our transition results for the three different inner cylinders along with historical data, incorporating the datasets from both Wendt (1933) and Taylor (1936) in addition to other observations having pure outer cylinder rotation. Where possible we include hysteresis measurements, where the (higher) transition $Re$ upon increasing ($Re_{cr}$) is distinguished from the inverse transition (i.e. relaminarization) upon decreasing $Re$. The new transition data is seen to fit well with previous observations and their inferred quadratic scaling above $\Delta R/R \geqslant 0.1$.

The scatter of transition $Re$ values seen in figure 2 has some significance. Owing to the finite-amplitude nature of the subcritical instability, perturbations of larger amplitude may trigger instability at lower $Re$. In our experiments, turbulence was sometimes inadvertently triggered prematurely for increasing $Re$ in instances where the flow was noticeably perturbed, e.g. due to a sudden acceleration, or the wake of a stray bubble. Similarly, we can see from the work of R. A. Bagnold (as summarized by Hunt *et al.* 2002) that the subcritical transition occurred at less than half of the expected $Re_{cr}$ based on gap width, from which we infer there were significant perturbations in his wide gap apparatus. Conversely, the careful work by Schultz-Grunow (1959) demonstrated that a precisely controlled experiment could achieve laminar flow at exceptionally high $Re$, extending $Re_{cr}$ by an order of magnitude or more. This result is analogous to pipe flow experiments that, through careful minimization of initial perturbations, can achieve laminar flow up to order $10^5$ instead

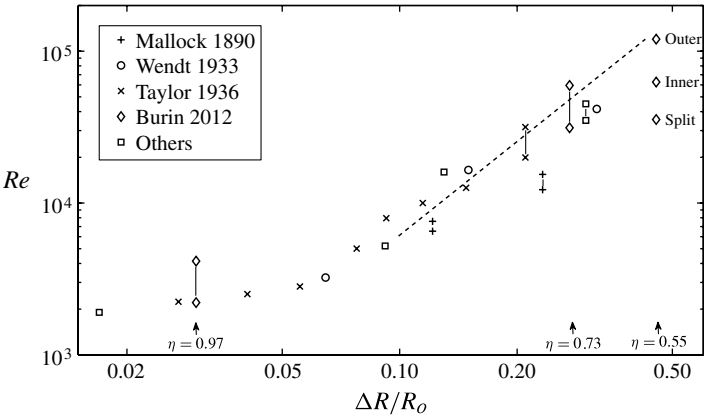


FIGURE 2. Transition *Re* as function of normalized gap width using both new and historical data. Note that $\Delta R/R_o = 1 - \eta$. Square data are from Couette (1890), Yamada & Imao (1986), Richard (2001) and Borrero-Echeverry, Schatz & Tagg (2010). Vertical lines represent hysteresis observations and the dashed trend-line denotes a squared dependence. For $\eta = 0.55$ the transition values are given using three different end-cap configurations.

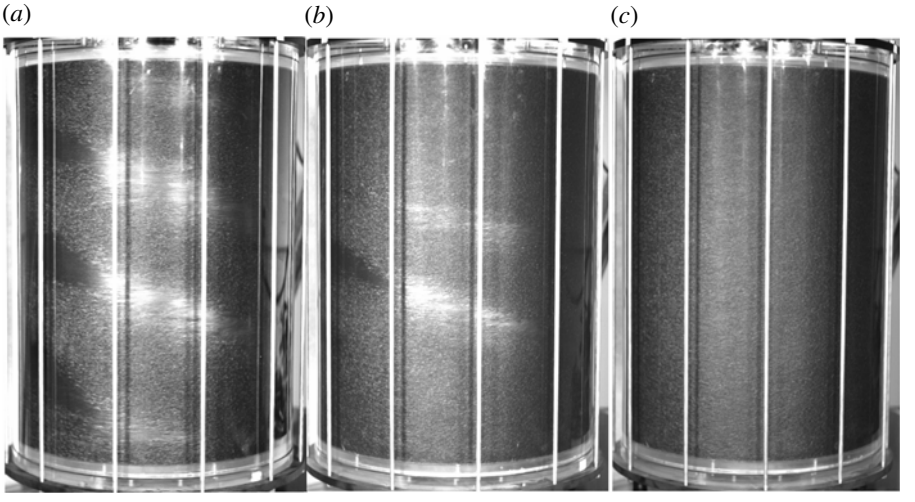


FIGURE 3. Transition imagery for the narrow gap case ($\eta = 0.97$) for *Re* increasing. Onset of turbulence is near $Re = 4500$. A mixed helicity phase at onset (not shown) eventually yields to a steady state of spiral turbulence (*a*). As *Re* increases further, turbulence spreads from the spiral bands; (*b*) is at $Re = 6500$. A fully turbulent state is reached by $Re = 7500$ (*c*).

of the usual 2–3000 (Pfenniger 1961). Interestingly, the transition values of Schultz-Grunow are in line with the others presented in figure 2 when he utilized an eccentric ($m = 1$) inner cylinder.

One of the useful features of the present apparatus is its transparent outer cylinder, allowing for spatiotemporal imaging of the subcritical transition. Figure 3 gives a sequence of time-independent images depicting the transition to turbulence for the $\eta = 0.97$ (i.e. narrow gap) case. Here we observe laminar flow until the onset of

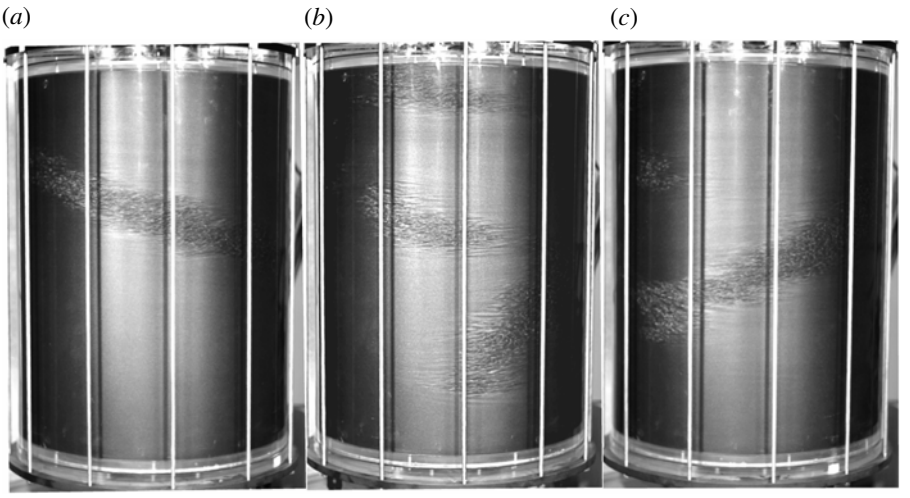


FIGURE 4. Transition imagery for the narrow gap case ($\eta = 0.97$) for $Re$ decreasing, where turbulent spots (sometimes extended) and single spirals (of either helicity) may be observed: (*a–c*) at $Re = 2500$, just above the relaminarization threshold $Re \approx 2000$.

spiral turbulence from a laminar state near $Re_{cr} = 4500$. Onset of the turbulence is typically initiated from the end-caps of the device and proceeds to create angled turbulent patches that eventually evolve (at the same $Re$) into spiral turbulence after about $\leqslant 1$ min. The final helicity of the spiral bands appears to be random with both states being observed with apparent equal probability. By further increasing $Re$ the turbulence spreads from the oblique bands until the flow is fully turbulent near $Re \approx 7500$. This process of becoming fully turbulent through an expansion of already-turbulent domain(s), as well as the observation of helicity switching, was reported in Coles (1965) and Andereck *et al.* (1986) for the case of counter-rotating cylinders, although these studies drove turbulence via $\Omega_i$.

Hysteresis is clearly evident in the subcritical transition. Turbulent features are generally maintained below $Re_{cr}$, but they become more intermittent in both time and space. The dominant spiral pattern tends to break up, allowing for both helicities of bands as well as for unconnected turbulent patches of varying degrees of pitch and elongation. This transition from spirals to patches for decreasing $Re$ has been seen in counter-rotating flow (Goharzadeh & Mutabazi 2001) and torsional Couette flow (Cros & Le Gal 2002), and more recently in rotating planar Couette flow (Tsukahara *et al.* 2010). Turbulent patches may occasionally join to form what appears to be a single spiral, and in some cases tend to form on one side of the previous turbulent patch in a process reminiscent of turbulent spot spreading over a flat plate (Elder 1960). This can happen a few times in succession, such that an oblique band is seen in piecemeal fashion over time. Representative images from this hysteretic regime for the narrow gap case are seen in figure 4. Complete relaminarization occurs near $Re \approx 2000$.

In contrast to the narrow gap transition, the subcritical transition for wider gaps ($\eta = 0.55$ and $0.73$) does not contain spiral turbulence, or even a similarly distinct intermediate phase for increasing $Re$. For the wider gaps the transition is usually observed to originate from the midplane of the cylinders, i.e. where the Ekman flows converge. For the narrow gap case turbulence always starts from one or both of the end-caps (although turbulence may start from the end-caps in wider gap flows as well

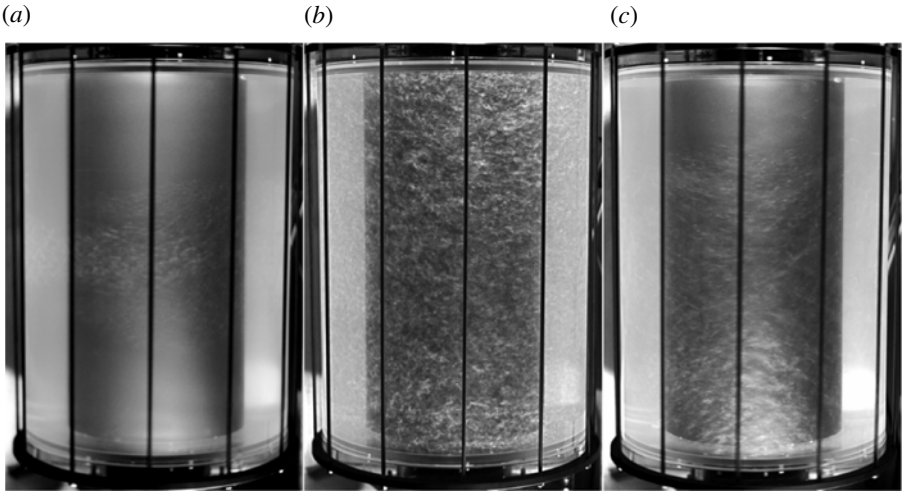


FIGURE 5. Transition imagery highlights from the widest gap case ($\eta = 0.55$). Near $Re = 70\,000$ turbulence breaks out from a midplane layer (*a*). The flow is fully turbulent near $Re = 100\,000$ (*b*). Hysteresis is evident down to $Re$ near 50 000 (*c*) with relatively large patches of intermittent turbulence. The radial location of the turbulence is dependent on the chosen end-cap configuration.

if the acceleration between flow speeds is not sufficiently quasi-static). After onset, and at the same $Re$, turbulence progresses to fill the entire annulus vertically, although not entirely in radius, as we discuss further below. As with the narrow gap case, hysteresis with turbulent patchiness is observed below $Re_{cr}$. Highlights of a transition sequence for the widest gap case ($\eta = 0.55$) are shown in figure 5.

Figure 6 (*a*) presents an integrated picture of the development of turbulence with $Re$ for the $\eta = 0.97$ case, using a spatially integrated parameter ($\gamma$) representing the fraction of the flow that appears turbulent. This fraction is estimated from an average of time-independent photographs of the illuminated side of the flow as depicted in figures 3 and 4. Note that adjusting the contrast of the photos, or other settings, does not significantly change the pixel count representing laminar and turbulent regions. Hysteresis is most evident below the $Re_{cr}$ of 4500 where the turbulence is generally patchy and not coherent as spirals. As discussed above, for increasing $Re$ the turbulence onset normally appears abruptly as spirals (after a transitory mixed helicity phase). These results may be compared with experimental results in both circular (Colovas & Andereck 1997; Goharzadeh & Mutabazi 2001) and planar Couette flows (Bottin & Chaté 1998), as well as to recent simulations (Dong & Zheng 2011).

We note that while our initial observations of hysteresis phenomena appear qualitatively similar to observations from other subcritical flows, additional data is needed to investigate the statistics associated with relaminarization, the boundary of which should be probabilistic (Borrero-Echeverry *et al.* 2010). Also much longer wait times are necessary: the viscous decay time, $\tau_\nu \approx (\Delta R)^2/\nu$ (Czarny & Lueptow 2007), is near 1 and 3 hours (respectively) for the $\eta = 0.73$ and 0.55 cases considered. However, initial hysteresis observations made with $\eta = 0.73$, allowing for a full viscous time, are similar to observations with significantly shorter wait times. We hope to address hysteresis and transition statistics more fully in a future study.

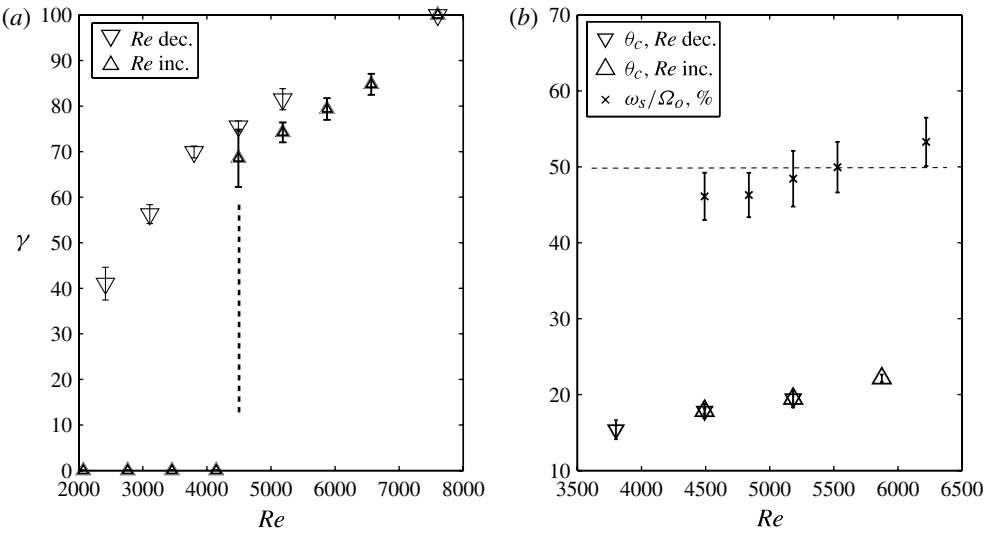


FIGURE 6. (*a*) Integrated turbulent fraction with *Re* for the narrow-gap case ($\eta = 0.97$), with evident hysteresis; (*b*) displays two basic properties of the spiral pattern: representative tilt angle ($\theta_c$) and azimuthal rotation rate ($\omega_s$), given as a percentage of outer cylinder rate ($\Omega_o$).

In figure 6 we also present a basic summary of spiral properties (*b*), including average pitch angle and the azimuthal rotation rate of the spiral pattern ($\omega_s$) as a function of *Re*. Both values appear to trend mildly upwards and approximately linearly with *Re*. Since pitch angle has been seen previously to vary significantly with axial distance from the end-caps (Hegseth *et al.* 1989), the data here is evaluated in just the central portion of the imaged area to emphasize its trend over *Re*. No significant hysteresis is observed in the spiral pitch with *Re*. In counter-rotating flow, $\omega_s$ has been observed to be approximately the mean of the two cylinder rotation rates ($\Omega_m$) below a *Re* of 10 000 (van Atta 1966). When normalized by $\Omega_o$, Andereck *et al.* (1986) found no dependence of this rate on $\Omega_i$. Similar results were obtained by Prigent (2001) who found $\omega_s \approx \Omega_m$ for a wide range of $\Omega_i$ and $\Omega_o$ values in counter-rotating flow. Our $\omega_s$ results also are near $\Omega_m$, which is just 50 % of $\Omega_o$, but also show a slight increase with $\Omega_o$. This increase may be due to the turbulent energy migrating outward in radius as it develops when *Re* is increased, as has been seen in recent simulations (Dong & Zheng 2011). Spiral turbulence was typically not seen in earlier circular Couette experiments due to the relatively large wavelength of the bands, $\lambda_z \approx 40$–$60\Delta R$. A similar geometrical relation was discovered empirically by Prigent *et al.* (2002, 2003), who found $\lambda_z \approx 20$–$40\Delta R$. We discuss this geometric relationship below after reviewing velocimetry results.

### 3.2. *Velocimetry*

In figure 7 we present time-averaged velocimetry results using LDV. A representative laminar and turbulent profile over normalized radius is given for each configuration. The difference between the narrow and wider gap cases is clear in a few respects. First, the departure from the laminar analytic solution increases with gap size, due to end effects upon the bulk flow. The shape of the turbulent profile also changes with gap size, though is similar for the $\eta = 0.55$ and 0.73 cases. The departure of the profiles from of the analytic Couette solution (Joseph 1976), which is significant

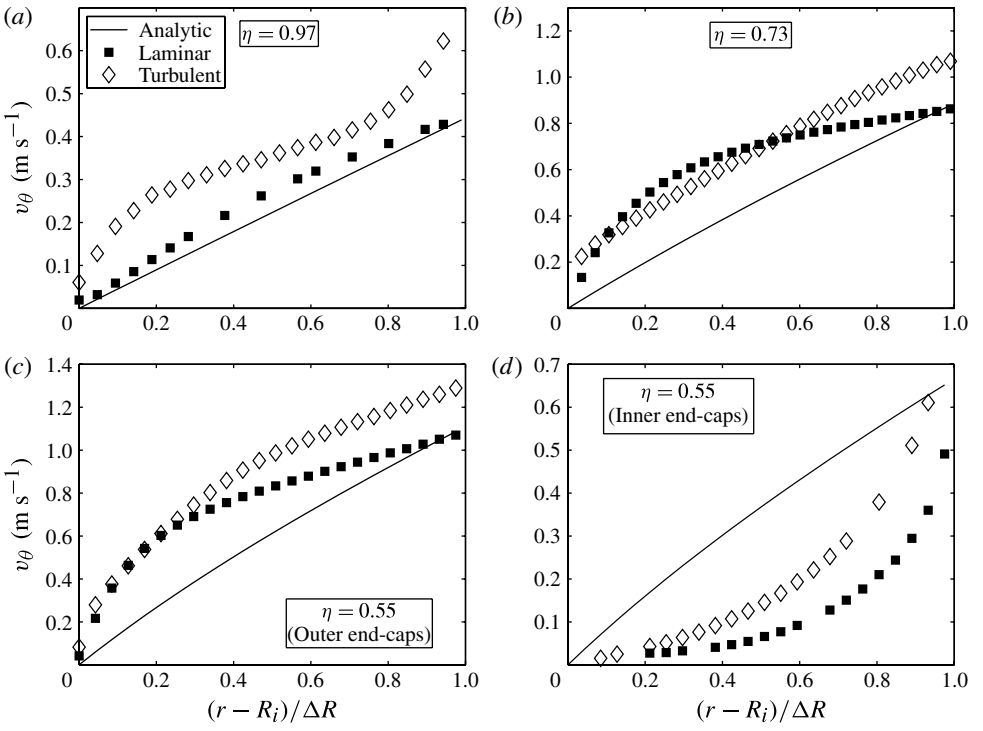


FIGURE 7. Velocimetry contrasting velocity distributions of mean azimuthal velocity over radius for different gap widths. Measurements are taken at $z = 6$ cm (depth, i.e. from the top of the apparatus) although are independent of height. Theoretical laminar (Couette) profiles are also given for comparison. Approximate *Re* for the profiles (based on (1.1)) are: 2800 and 6800 for $\eta = 0.97$; 50 000 and 65 000 for $\eta = 0.73$; 100 000 and 130 000 for $\eta = 0.55$ (outer); and 65 000 and 100 000 for $\eta = 0.55$ (inner).

for wider gaps or shorter $\Gamma$, is discussed in Coles & Atta (1966) along with their $z$ independence, which can be maintained in short $\Gamma$ flows via stronger, although still thin, end-cap boundary (Ekman) layers.

In general the shape of the profiles for each gap width (whether laminar or turbulent) do not change up to $2Re_{cr}$, which is the approximate maximum *Re* of this study. The profile for the intermediate case of spiral turbulence in the $\eta = 0.97$ case is also nearly indistinguishable from more fully turbulent profiles at higher *Re*. We note that this narrow gap case is unique in having an inflection point due to the proximity of the sidewalls to each other, an issue we will return to in the discussion below. Different end-cap conditions (unique to the $\eta = 0.55$ case) also clearly affect the flow profile and consequently $Re_{cr}$.

The radial distribution of turbulent fluctuation energy (as reflected in the time-averaged azimuthal root mean square velocity) varies considerably with gap width, as can be seen in figure 8. The narrow-gap case features turbulent fluctuations near 10 % filling most of the annular domain for both spiral turbulence and fully developed turbulence. The wider gap cases on the other hand contain relatively less fluctuation energy, being ∼10 % only near the inner cylinder and then decaying outward, reaching low levels (≈1 %) near the outer cylinder. Indeed, visualization with Kalliroscope

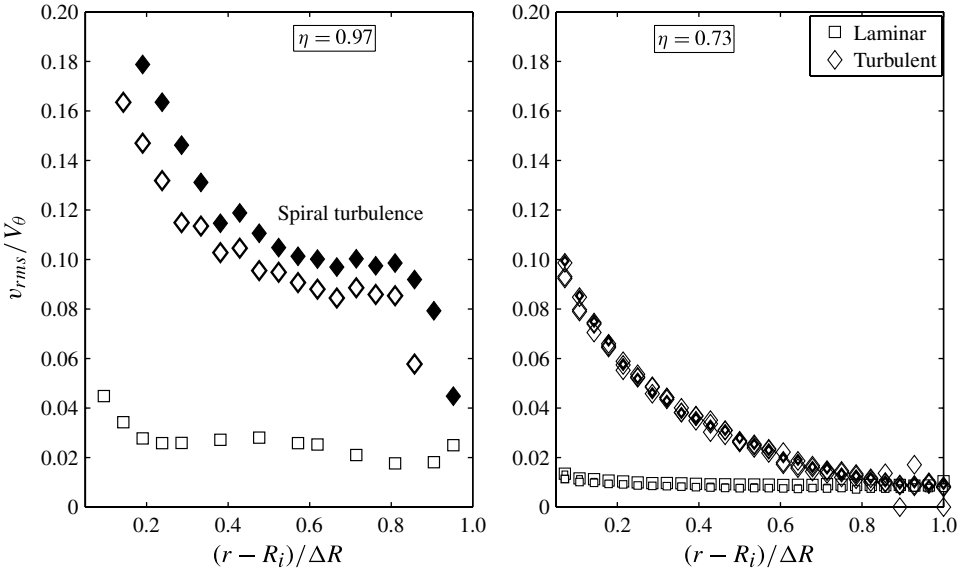


FIGURE 8. Radial distributions of normalized fluctuations. Here $Re$ and $z$ are the same as in figure 7, with additional $Re$ shown for $\eta = 0.97$ ($Re = 4500$) for spiral turbulence and for $\eta = 0.73$ ($Re = 75\,000$, $100\,000$ and $125\,000$) to illustrate $Re$ independence once turbulent.

indicates that an outer layer of fluid in these cases is apparently laminar. This radial decay is most pronounced when the outer end-caps rotate with the outer cylinder. For $\eta = 0.55$, when end-caps that are wholly coupled to the inner cylinder are used, there is more absolute fluctuation energy at larger radii, but the same trend of outward decay prevails upon normalization due to very small mean speeds throughout the inner half of the gap for this configuration. Once turbulent, both the radial distribution and magnitude of the relative fluctuations do not appear to change significantly with $Re$ for any gap size.

## 4. Discussion

In conclusion we briefly discuss two of the principal results of our initial study. The first concerns the localized nature of the shear and the role played by the end-caps. The second concerns spiral turbulence, which is observed only using a narrow gap.

### 4.1. *On the importance of localized shear*

Figures 7 and 8 considered together suggest that turbulent fluctuations originate and are confined to regions of sufficient shear. This correlation is seen in figure 9. Note that the narrow gap case features significantly higher rates of shear along with double-peaked fluctuation and shear profiles, which are due to the overlapping sidewall boundary layers. This profile shape was observed in earlier measurements (Yamada & Imao 1986) and also inferred in recent simulations of spiral turbulence in counter-rotating flow (Dong & Zheng 2011). The wider gap cases by contrast are monotonic due to their shear profile having only one maximum, which is found near the inner cylinder when the end-caps are coupled to the outer cylinder.

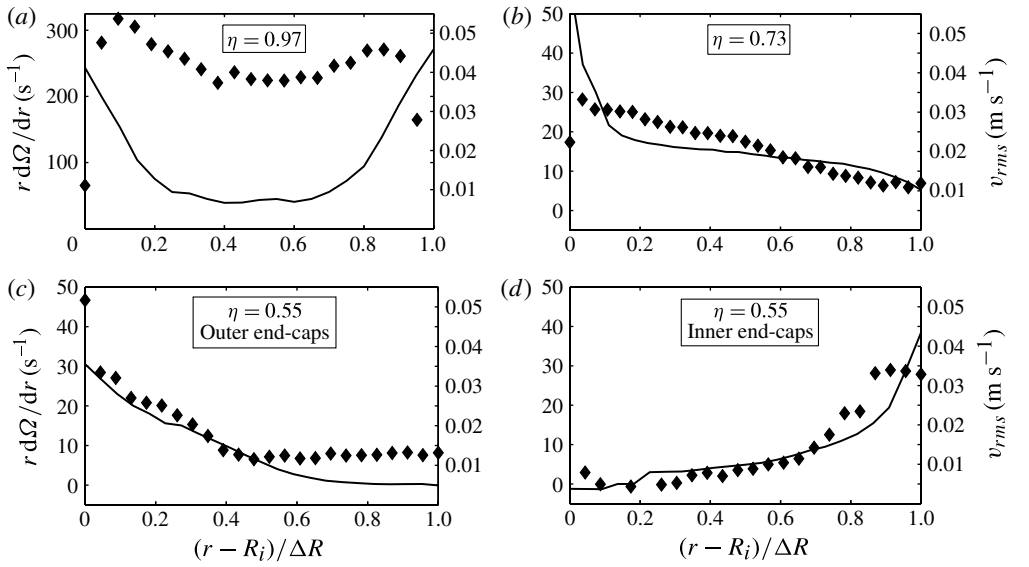


FIGURE 9. Radial distribution of mean shear (smoothed line) and azimuthal velocity fluctuations (diamonds) showing correlation. These distributions are derived directly from the turbulent profiles given in figures 7 and 8.

Our results with the widest gap case ($\eta = 0.55$; see ($c$, $d$) of figures 7 and 9) make it clear that the end-cap conditions can significantly affect the bulk flow, primarily by determining the radial location of the shear layer(s). End-caps that rotate with the outer cylinder produce a more stable flow ($Re_{cr} \approx 120\,000$) than when they are coupled to the inner cylinder ($Re_{cr} \approx 60\,000$). A split configuration will transition at even lower $Re$, with $Re_{cr} \approx 30\,000$. (We conjecture that the split configuration is the most unstable of the three configurations due to its shear layer being free, away from the viscous boundaries.) We note that this disparity of $Re_{cr}$ for differing end-cap conditions was not noticed by Wendt (1933); but this is understandable given that his flows had a free upper surface, and were thus less subject to end-effects.

The difference in apparent stability between the outer and inner end-cap configurations can be understood in light of the radius of curvature at the shear layer. Shearing is localized near the inner cylinder in the former case, i.e. at the location of highest curvature, a condition generally associated with a larger stabilizing influence (So & Mellor 1973). In fact, if we replace $R_o$ with the approximate radial location of the shear layer in the numerator of $Re$ in (1.1) we find that the inner and outer end-cap configurations transition at nearly the same $Re \approx 60$–$70\,000$. A systematic investigation of this coincidence (e.g. by incrementally moving the shear layer location in radius) is unfortunately not possible with our apparatus.

Considering the localized nature of the shear and turbulence in the wider gaps, it seems appropriate to revisit the notion of a global Reynolds number for this system. Besides current data we recall similar experiments by Dunst (1972) in a very wide gap ($\eta = 0.1$, with a free surface), who observed shear flow only very near the inner cylinder, with the rest of the flow moving as a solid body. This large unsheared region found in large gaps is not dynamically important to the shear-driven transition, which is understood to be local in nature.

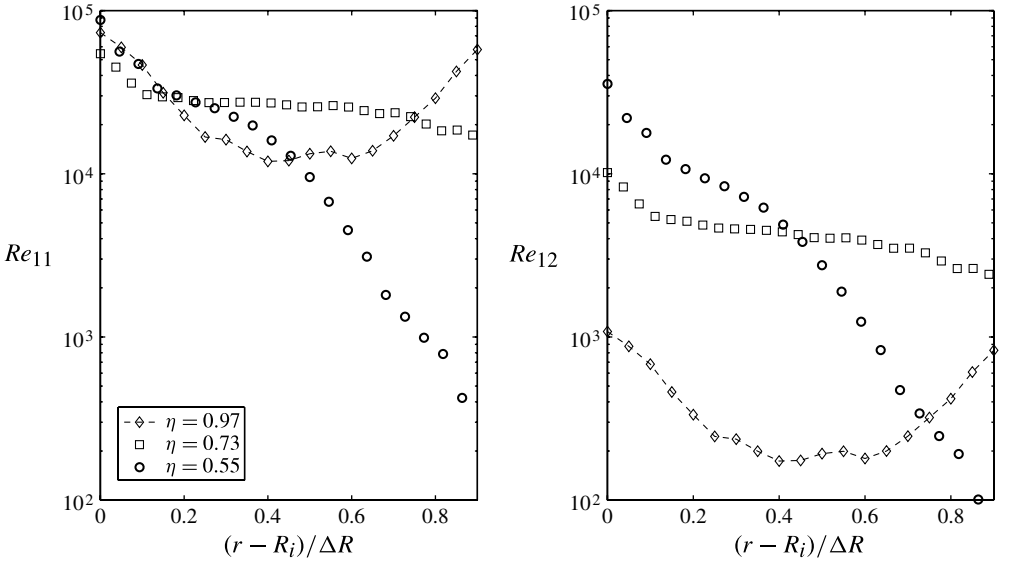


FIGURE 10. Localized Reynolds numbers over normalized radius (4.2) and (4.3) for turbulent profiles with $Re_{cr} < Re < 1.5Re_{cr}$.

A Reynolds number based on the shear averaged over the gap width is given by Barkley & Tuckerman (2007) as

$$Re^{TC} = \frac{(R_i\Omega_i - \eta R_o\Omega_o)}{(1+\eta)d}\frac{d^2}{\nu} \tag{4.1}$$

where $d = \Delta R/2$; a similar formulation was given by Manneville (2004). If we modify this expression to account for the local shear rate $r\,\mathrm{d}\Omega/\mathrm{d}r$, we may arrive at either

$$Re_{l1} = \frac{\eta}{1+\eta}\frac{r^2(\mathrm{d}\Omega/\mathrm{d}r)d}{\nu} \tag{4.2}$$

or

$$Re_{l2} = \frac{\eta}{1+\eta}\frac{r(\mathrm{d}\Omega/\mathrm{d}r)d^2}{\nu} \tag{4.3}$$

where $Re_{l1}$ emphasizes the local radius $r$ while $Re_{l2}$ emphasizes the half gap $d$. Either equation is permissible, at least from a dimensional standpoint.

The localized expressions for $Re$ above are given over normalized radius in figure 10 for turbulent profiles just above the transition threshold ($Re_{cr} < Re < 1.5Re_{cr}$). Several aspects of the data are worth noting. Considering first $Re_{l1}$, we see that near the inner cylinder the values are quite similar (50 000–90 000). The contrast with $Re$ as commonly defined (1.1) is greatest for $\eta = 0.97$, where a larger shear rate and inner cylinder radius compensates for the small gap width. Near the outer cylinder we find that $\eta = 0.97$ has the largest $Re_{l1}$, while $\eta = 0.55$ has the smallest; this apparent reversal in stability is sensible given the low shear rates and fluctuation levels found in the outer layers of the larger gap flows. Values of $Re_{l2}$ near the inner cylinder are similar in value (and ordering in $\eta$) to those found in figure 2 which uses (1.1).

The $\eta = 0.97$ case given in figure 10 corresponds to spiral turbulence. Here $Re^{TC} = 1000$, while it can be seen that within the central gap $Re_{l2} \approx 200$. Interestingly, a radial average from $0.1 \leqslant (r - R_i)/\Delta R \leqslant 0.9$ yields $Re_{l2} = 335$, a value consistent with the average of $Re^{TC}$ given in Barkley & Tuckerman (2007) in their comparison of spiral turbulence limits in various shear flows. A local evaluation of $Re$ may thus be preferable even for narrow gaps.

### 4.2. *On the origin of spiral turbulence*

The qualitative difference between the transition sequences in the narrow and wider gaps seems especially significant considering the presence of spiral turbulence in the former. Though all wall-bounded shear flows can produce intermittent turbulent structures, the regular alternating bands of spiral turbulence appear to be unique to quasi-two-dimensional shear flows, including planar, circular, and torsional Couette flow, in addition to Poiseuille channel flow. The turbulent patches observed in pipe flows (puffs, slugs) and single boundary layers (Emmons spots) apparently do not form the oblique banded pattern.

In the experiments by Cros & Le Gal (2002) between a stationary and rotating disc, the pattern shifts from turbulent spots to turbulent spirals for the same $Re$ (based on disc radius) if the spacing between the discs is reduced. If one instead assumes that the proper $Re$ for this experiment should include the inter-disc spacing as a length scale, then the transition from spots to spirals occurs for decreasing $Re$, i.e. opposite the normal direction. Either consideration hints at the possible role of an interaction between opposing boundary layers in producing the banding. The interaction process that produces spiral turbulence, presumably between the largest scales of the outer boundary layers, could be similar in nature to the phase locking that occurs at the sheared interface between coaxial jets (Dahm, Frieler & Tryggvason 1992).

In any case, in light of our results, the empirical requirement $H \gg \Delta R$ may perhaps be understood not only as a necessary *removed distance* of the end-caps ($\Gamma \to \infty$), but as a *necessary closeness* of the sidewalls of the cylinders, the boundary layers of which appear to overlap somewhat under the conditions of spiral turbulence. That is, we consider the geometrical relation that allows for spiral wavelengths ($H > \lambda_z$) to be a necessary but not sufficient condition for shear-driven spiral turbulence.

In wider gap flows, where intermittent turbulence can be seen, but the regular banding associated with spiral turbulence is never observed (as with single boundary layers) the bulk flow remains largely unaffected. We suppose then that spiral turbulence could be formed through an interaction between opposing boundary layers, and propose a rudimentary banding criterion $\Delta R \approx 2\delta$, where $\delta$ is the approximate boundary layer thickness. When $\Delta R \ll 2\delta$ viscous processes overcome shear, and when $\Delta R \gg 2\delta$ a relatively inviscid core effectively separates boundary layers, preventing interaction. An experimental test of this conjecture would be to generate shear-driven turbulence in a Taylor–Couette apparatus that has a velocity profile dominated by a single shear layer (as in the $\eta = 0.55$ or 0.73 profiles seen in figure 7). If the apparatus can be made adequately tall, with $H \geqslant 40\Delta R$ (noting that a change in $H$ leaves $Re$ unaffected), one may see whether spiral turbulence depends only on sufficient shear and apparatus height.

## Acknowledgements

We would like to thank the shop personnel at Scripps Institute of Oceanography (SIO/UCSD), especially D. Malmberg and J. Galipeau, for engineering work on the apparatus; also D. L. Defoor for his initial work on its motor control system, and

Measurement Sciences Inc. (Pasadena, CA) for providing a LDV diagnostic. We also thank P.-Y. Longaretti for reviewing an early version of the manuscript, and an anonymous reviewer who helped clarify several points. This research was partially supported by a Cottrell College Science Award from the Research Corporation for Science Advancement (RCSA).

## REFERENCES

ANDERECK, C. D., LIU, S. S. & SWINNEY, H. 1986 Flow regimes in a circular Couette system with independently rotating cylinders. *J. Fluid Mech.* **164**, 155–183.

VAN ATTA, C. 1966 Exploratory measurements in spiral turbulence. *J. Fluid Mech.* **25**, 495–512.

BARKLEY, D. & TUCKERMAN, L. S. 2007 Mean flow of turbulent-laminar patterns in plane Couette flow. *J. Fluid Mech.* **576**, 109–137.

BORRERO-ECHEVERRY, D., SCHATZ, M. F. & TAGG, R. 2010 Transient turbulence in Taylor–Couette flow. *Phys. Rev.* E **81**, 025301.

BOTTIN, S. & CHATÉ, H. 1998 Statistical analysis of the transition to turbulence in plane Couette flow. *Eur. Phys. J.* B **6**, 144–155.

BURIN, M. J., JI, H., SCHARTMAN, E., CUTLER, R., HEITZENROEDER, P., LIU, W., MORRIS, L. & RAFTOPOLOUS, S. 2006 Reduction of Ekman circulation within Taylor–Couette flow. *Exp. Fluids* **40**, 962–966.

COLES, D. 1965 Transition in circular Couette flow. *J. Fluid Mech.* **21**, 385–425.

COLES, D. & VAN ATTA, C. 1966 Measured distortion of a laminar circular Couette flow by end effects. *J. Fluid Mech.* **25**, 513–521.

COLOVAS, P. W. & ANDERECK, C. D. 1997 Turbulent bursting and spatiotemporal intermittency in the counterrotating Taylor–Couette system. *Phys. Rev.* E **55**, 2736–2741.

COUETTE, M. M. 1890 Etudes sur le frottement des liquides. *Ann. Chim. Phys.* **6**, 433–510.

COUGHLIN, K. & MARCUS, P. S. 1996 Turbulent bursts in Couette–Taylor flow. *Phys. Rev. Lett.* **77**, 2214–2217.

CROS, A. & LE GAL, P. 2002 Spatiotemporal intermittency in the torsional Couette flow between a rotating and a stationary disk. *Phys. Fluids* **14**, 3755–3765.

CZARNY, O. & LUEPTOW, R. 2007 Time scales for transition in Taylor–Couette flow. *Phys. Fluids* **19**, 054103.

DAHM, W. J. A., FRIELER, C. E. & TRYGGVASON, G. 1992 Vortex structure and dynamics in the near field of a coaxial jet. *J. Fluid Mech.* **241**, 371–402.

DAVIAUD, F., HEGSETH, J. & BERGÉ, P. 1992 Subcritical transition to turbulence in plane Couette flow. *Phys. Rev. Lett.* **69**, 054103.

DONG, S. 2009 Evidence for internal structures of spiral turbulence. *Phys. Rev.* E **80**, 067301.

DONG, S. & ZHENG, X. 2011 Direct numerical simulation of spiral turbulence. *J. Fluid Mech.* **668**, 150–173.

DUBRULLE, B., DAUCHOT, O., DAVIAUD, F., LONGRETTI, P.-Y, RICHARD, D. & ZAHN, J.-P. 2005 Stability and turbulent transport in Taylor–Couette flow from analysis of experimental data. *Phys. Fluids* **17**, 095103.

DUGUET, Y., SCHLATTER, P. & HENNINGSON, D. S. 2010 Formation of turbulent patterns near the onset of transition in plane Couette flow. *J. Fluid Mech.* **650**, 119–129.

DUNST, M. 1972 An experimental and analytical investigation of angular momentum exchange in a rotating fluid. *J. Fluid Mech.* **55**, 301–310.

ECKHARDT, B., GROSSMANN, S. & LOHSE, D. 2007 Torque scaling in turbulent Taylor–Couette flow between independently rotating cylinders. *J. Fluid Mech.* **581**, 221–250.

ELDER, J. W. 1960 An experimental investigation of turbulent spots and breakdown to turbulence. *J. Fluid Mech.* **9**, 235–246.

VAN GILS, D. P. M., HUISMAN, S., BRUGGERT, G.-W., SUN, C. & LOHSE, D. 2011 Torque scaling in turbulent Taylor–Couette flow with co- and counter-rotating cylinders. *Phys. Rev. Lett.* **106**, 024502.

GOHARZADEH, A. & MUTABAZI, I. 2001 Experimental characterization of intermittency regimes in the Couette-Taylor system. *Eur. Phys. J.* B **19**, 157–162.

HASHIMOTO, S., HASOBE, A., TSUKAHARA, T., KAWAGUCHI, Y. & KAWAMURA, H. 2009 An experimental study on turbulent-stripe structure in transitional channel flow. In *Proceedings of the Sixth International Symposium on Turbulence, Heat and Mass Transfer, Rome, Italy*, pp. 193–196.

HEGSETH, J. J., ANDERECK, C. D., HAYOT, F. & POMEAU, Y. 1989 Spiral turbulence and phase dynamics. *Phys. Rev. Lett.* **62**, 257–260.

VAN HOUT, R. & KATZ, J. 2011 Measurements of mean flow and turbulence characteristics in high-Reynolds number counter-rotating Taylor–Couette flow. *Phys. Fluids* **23**, 105102.

HUNT, M. L., ZENIT, R., CAMPBELL, C. S. & BRENNEN, C. E. 2002 Revisiting the 1954 suspension experiments of R. A. Bagnold. *J. Fluid Mech.* **452**, 1–24.

JI, H., BURIN, M. J., SCHARTMAN, E. & GOODMAN, J. 2006 Hydrodynamic turbulence cannot transport angular momentum effectively in astrophysical disks. *Nature* **444**, 343.

JOSEPH, D. D. 1976 *Stability of Fluid Motions*. Springer-Verlag.

LESUR, G. & LONGARETTI, P.-Y. 2005 On the relevance of subcritical hydrodynamic turbulence to accretion disk transport. *Astron. Astrophys.* **444**, 25–44.

MALLOCK, A. 1896 Experiments on fluid viscosity. *Proc. R. Soc. Lond.* **45**, 126–132.

MANNEVILLE, P. 2004 Spots and turbulent domains in a model of transitional plane Couette flow. *Theor. Comput. Fluid Dyn.* **18**, 169–181.

MESEGUER, A., MELLIBOVSKY, F., AVILA, M. & MARQUES, F. 2009 Instability mechanisms and transition scenarios of spiral turbulence in Taylor–Couette flow. *Phys. Rev.* E **80**, 046315.

PAOLETTI, M. S. & LATHROP, D. P. 2011 Angular momentum transport in turbulent flow between independently rotating cylinders. *Phys. Rev. Lett.* **106**, 024501.

PFENNIGER, W. 1961 Transition in the inlet length of tubes at high Reynolds numbers.. In *Boundary Layer and Flow Control* (ed. G. V. Lachman). pp. 970–980. Pergamon.

PRIGENT, A. 2001 La spirale turbulente : motif de grande longueur donde dans les écoulements cisaillés turbulents. PhD thesis, Univ. Paris Sud, Orsay, France.

PRIGENT, A., GRÉGOIRE, G., CHATÉ, H. & DAUCHOT, O. 2003 Long-wavelength modulation of turbulent shear flows. *Physica* D **174**, 100–113.

PRIGENT, A., GRÉGOIRE, G., CHATÉ, H., DAUCHOT, O. & SAARLOOS, W. V. 2002 Large-scale finite-wavelength modulation within turbulent shear flows. *Phys. Rev. Lett.* **89**, 014501.

RICHARD, D. 2001 Instabilités hydrodynamiques dans les écoulements en rotation différentielle. PhD thesis, Univ. Paris 7 Denis Diderot, Paris, France.

RICHARD, D. & ZAHN, J.-P. 1999 Turbulence in differentially rotating flows. *Astron. Astrophys.* **347**, 734–738.

ROLLAND, J. & MANNEVILLE, P. 2011 Ginzburg–Landau description of laminar-turbulent oblique band formation in transitional plane Couette flow. *Eur. Phys. J.* B **80**, 529–544.

SCHARTMAN, E., JI, H. & BURIN, M. J. 2009 Development of a Couette–Taylor flow device with active minimization of secondary circulation. *Rev. Sci. Instrum.* **80**, 024501.

SCHULTZ-GRUNOW, F. 1959 Zur Stabilität der Couette–Strömung. *Z. Angew. Math. Mech.* **39**, 101–110.

SO, R. M. C. & MELLOR, G. 1973 Experiment on convex curvature effects in turbulent boundary layers. *J. Fluid Mech.* **60**, 43–62.

TAYLOR, G. I. 1923 Stability of a viscous liquid contained between two rotating cylinders. *Phil. Trans. R. Soc. Lon.* A **223**, 289–343.

TAYLOR, G. I. 1936 Fluid friction between rotating cylinders. I. Torque measurements. *Proc. Roy. Soc. Lond.* A **157**, 546–564.

TSUKAHARA, T., TILLMARK, N. & ALFREDSSON, P. H. 2010 Flow regimes in a plane Couette flow with system rotation. *J. Fluid Mech.* **648**, 5–33.

TUCKERMAN, L. & BARKLEY, D. 2011 Patterns and dynamics in transitional plane Couette flow. *Phys. Fluids* **23**, 041301.

WENDT, F. 1933 Turbulente Strömungen zwischen zwei rotierenden konaxialen Zylindern. *Ing.-Arch.* **4**, 577–595.

YAMADA, Y. & IMAO, S. 1986 Flow of a fluid contained between concentric cylinders both rotating. *Bull. Japan Soc. Mech. Eng.* **29**, 1691–1697.

ZELDOVICH, Y. B. 1981 On the friction of fluids between rotating cylinders. *Proc. R. Soc. Lond.* A **374**, 299–312.